Cell Communication and Signaling

RESEARCH

Open Access

RNA-binding protein HuR inhibition induces multiple programmed cell death in breast and prostate cancer

Lanjing Wei[1,2], Sung Hae Kim[3], Ahlam M. Armaly[4], Jeffrey Aubé[4], Liang Xu[3,5,6*] and Xiaoqing Wu[3,5*]

Abstract

The RNA-binding protein Hu antigen R (HuR) plays a pivotal role in cancer progression, and previous studies have demonstrated its involvement in suppressing cell death in cancer. However, the precise mechanisms underlying HuR inhibition-induced cell death remain elusive. Here, we investigated the impacts of HuR functional inhibition via the small molecule inhibitor KH-3 on cell proliferation, colony formation, and cell death across multiple cancer cell lines, with an emphasis on breast and prostate cancers. KH-3 treatment induced apoptotic cell death of various cancer cell lines, as well as autophagy-associated cell death and ferroptosis. Remarkably, KH-3-induced cell death was partially rescued by an autophagy inhibitor and a ferroptosis inhibitor. The anti-tumor effects of KH-3 were further validated in two mouse xenograft models of human prostate cancer. Mechanistically, KH-3 reduced the expression of HuR targets involved in apoptosis and ferroptosis suppression, including cFLIP and SLC7A11, respectively. Moreover, cFLIP silencing enhanced Caspase-8 activation as well as PARP cleavage in both breast cancer and prostate cancer cells. Both KH-3-induced pharmacological HuR inhibition and RNA interference-mediated HuR knockdown reduced the expression of SLC7A11. Additionally, KH-3 also reduced XIAP and Survivin, enhancing the activation of multiple caspases and leading to apoptosis. This study highlights the critical roles of HuR in programmed cell death regulation, advocating HuR inhibition as a promising anti-tumor strategy for cell-death-inducing cancer therapy.

Keywords HuR, Cell death, Breast cancer, Prostate cancer, Mouse tumor models

*Correspondence:
Liang Xu
xul@ku.edu
Xiaoqing Wu
wuxq@ku.edu
[1] Bioengineering Program, The University of Kansas, Lawrence, KS 66045-7534, USA
[2] Present Address: Department of Medical Oncology, Dana-Farber Cancer Institute, Boston, MA 02215, USA
[3] Department of Molecular Biosciences, The University of Kansas, Lawrence, KS 66045-7534, USA
[4] Division of Chemical Biology and Medicinal Chemistry, UNC Eshelman School of Pharmacy, The University of North Carolina, Chapel Hill, NC 27599, USA
[5] The University of Kansas Cancer Center, The University of Kansas Medical Center, Kansas City, KS 66160, USA
[6] Department of Radiation Oncology, The University of Kansas Medical Center, Kansas City, KS 66160, USA

Background

The RNA-binding protein Hu antigen R (HuR), also known as ELAVL1 (embryonic lethal, abnormal vision, Drosophila-like protein 1), is a well-characterized human RNA binding protein associated with breast cancer [1]. HuR binds to the U-and AU-rich elements (AREs), predominantly located in the 3'-untranslated region (UTR) and occasionally in the 5'-UTR of target mRNAs [2]. Through binding to target mRNAs using three RNA-recognition-motifs (RRMs) [3, 4], HuR post-transcriptionally regulates the mRNAs, leading to various effects such as mRNA stabilization, upregulation of translation, and inhibition of translation of certain target mRNAs [2]. By interacting with target mRNAs, HuR promotes the

© The Author(s) 2024. **Open Access** This article is licensed under a Creative Commons Attribution-NonCommercial-NoDerivatives 4.0 International License, which permits any non-commercial use, sharing, distribution and reproduction in any medium or format, as long as you give appropriate credit to the original author(s) and the source, provide a link to the Creative Commons licence, and indicate if you modified the licensed material. You do not have permission under this licence to share adapted material derived from this article or parts of it. The images or other third party material in this article are included in the article's Creative Commons licence, unless indicated otherwise in a credit line to the material. If material is not included in the article's Creative Commons licence and your intended use is not permitted by statutory regulation or exceeds the permitted use, you will need to obtain permission directly from the copyright holder. To view a copy of this licence, visit http://creativecommons.org/licenses/by-nc-nd/4.0/.

expression of proteins involved in multiple major cancer traits, including resistance to cell death [5].

There are three main types of cell death: apoptosis, necrosis, and autophagy-associated cell death [6] and each mode of cell death exhibits distinct characteristics and mechanisms. In addition to these well-established types of cell death, other forms have been identified and characterized, such as pyroptosis [7], necroptosis [8], ferroptosis [9], NETosis [10], and disulfidptosis [11].

HuR plays critical roles in suppressing apoptotic cell death by stabilizing the mRNA transcripts that encode anti-apoptotic proteins, such as BCL2, and MCL1 [4], as well as proteins suppressing pro-apoptotic proteins protein, such as PIM1, which phosphorylates and inactivates apoptotic effector BAD [12]. Moreover, HuR also inhibits the translation of apoptosis-associated proteins, such as Caspase-2, through the negative interference with internal ribosome entry site (IRES)-mediated translation [13]. Knockdown of HuR using RNA interference sensitizes adenocarcinoma cells [14] and colorectal cancer cells [15] to apoptosis by negatively regulating Caspase-2. Additionally, HuR knockout in mice leads to the death of mice in embryogenesis [16]. Despite these observations, how HuR interferes with the interplay between different cell death pathways and characteristics as well as mechanisms underlying HuR inhibition-induced cell death remain incompletely understood.

Furthermore, HuR may influence cell death by interacting with target mRNAs that are involved in multiple cell death modes. The proteins encoded by these mRNAs play crucial roles in regulating multiple cell death pathways and facilitating the crosstalk between different types of cell death pathways. The X-linked inhibitor of apoptosis protein (XIAP) has been identified as a HuR target [17]. XIAP inhibits the activity of Caspse-9, Caspase-7, and Caspase-3 and promotes the degradation of caspases via ubiquitinating them [18]. Similarly, HuR interacts with the 3'-UTR of Survivin mRNA, leading to an increase in the protein level of Survivin [19], which in turn inhibits Caspase-9, -7, and -3 [20]. Additionally, HuR stabilizes the mRNA encoding BCL2 [5], which suppresses intrinsic apoptotic cell death [21], and inhibits necroptosis [22]. BCL2 negatively regulates autophagy by preventing the formation of the pre-autophagosomal structure through its interaction with Beclin 1 [23]. Moreover, a recent investigation has shown that in gastric cancer cells, HuR binds to and enhances the stability of the mRNA transcript encoding for the solute carrier family 7 member 11 protein (SLC7A11) [24], also known as xCT or CCBR1, which protects cells from ferroptosis [9].

In addition, one study proposed that in pancreatic cancer cells, HuR interacts with the mRNA encoding the cellular FLICE-like inhibitory protein (cFLIP), and silencing HuR diminishes the mRNA stability of this protein [25]. The protein cFLIP acts as a regulator of apoptosis, necroptosis, and autophagy [26, 27]. cFLIP exerts its regulatory functions in an isoform-specific manner, affecting both apoptosis and necroptosis [27]. Both heterodimers formed between procaspase-8 and $cFLIP_L$ (the long form) or $cFLIP_S$ (the short form) function to inhibit the activation of Caspase-8, thereby suppressing apoptosis [26, 27]. Furthermore, it has been reported that cFLIP inhibits autophagy by preventing the binding of Atg3 to LC3 [28]. One recent study discovered that HuR is required for TNF and IFNγ-induced cell death by enhancing the mRNA stability and translation of Caspse-8 [29]. Despite these findings, the understanding of the relationship between HuR and cFLIP remains limited.

Our group recently reported that HuR functional inhibition using a small molecule inhibitor, KH-3, induces intrinsic apoptosis in human triple-negative breast cancer (TNBC) cells through the downregulation of BCL2 [30]. However, caspase inhibitors only partially rescued cells from KH-3-induced cell death [30]. It remains unclear whether KH-3 induces other types of cell death. On the other hand, multiple HuR targets have been reported to be implicated in the regulation of various forms of cell death, including apoptosis, necroptosis, and ferroptosis [4, 12, 13, 24, 27]. However, the role of HuR in regulating programmed cell death in cancer cells remains poorly understand. Therefore, in this study, we evaluated and validated the anti-cancer effects of KH-3 and the induced apoptosis in various cancer cell types. We then investigated whether HuR inhibition engaged with other modes of cell death. Furthermore, we sought to elucidate the signaling axis through which HuR regulates cell death.

Materials and methods

Cell culture and reagents

The following cell lines PC-3, DU145, C4-2B, MDA-MB-231, MCF7, EMT6, HCT116, and LNCaP, were purchased from the American Type Culture Collection (Manassas, VA). 2LMP is a subclone generated from MDA-MB-231 formed lung metastasis and was kindly provided by Dr. Marc Lippman [31]. Cells were cultured in DMEM (Corning, cat# 10–017-CV), RPMI-1640 (Corning, cat# 10–041-CV) (for LNCaP), or Waymouth's MB 752/1 medium (Gibco, cat# 11,220–035) (for EMT6) supplemented with 10% (v/v) fetal bovine serum (FBS, Sigma Aldrich, cat# F4135), 5% (v/v) L-glutamine (Corning, cat# 25–005-CI), and 1% (v/v) penicillin–streptomycin (Corning, cat# 30–002-CI). Cells were maintained as described in a humidified CO2 incubator at 37℃ with 5%

CO2 and used at low generation numbers. Cell lines utilized in this study were regularly monitored to ensure the mycoplasma-free cells. All the reagents utilized in this study were summarized in Supplementary Table 1.

RNA and protein extraction

After the indicated treatments, cells were harvested for RNA extraction using the TRIzol Reagent (Life Technologies, cat# 15,596) following the manufacturer's protocol. Both attached and detached cells were collected, washed twice with the pre-cold PBS buffer, and subjected to protein extraction using the RIPA buffer, following the protocol described before [30]. Tumor tissues of PC-3 xenografts in this study and MDA-MB-231 xenografts treated by KH-3 for four weeks [30] were processed for Western Blot following the same protocol.

RT-qPCR

The total RNA was reversely transcribed into cDNA using the commercial High Capacity cDNA Reverse Transcription Kit (AppliedBiosystems, cat# 4,368,813) following the manufacturer's protocol. The abundance of mRNA was examined using the PowerUP SYBR Green Master Mix kit (AppliedBiosystems, cat# A25742) on the StepOnePlus Real-Time PCR system (Applied Biosystems). The relative quantification of mRNA normalized to the *GAPDH* was performed using the ΔΔCt assay. All the primers used in this study are listed in Supplementary Table 2.

MTT-based cytotoxicity assay

Suspended cells in 200 μL medium containing KH-3 or vehicle control were seeded into a 96-well plate. After maintaining the cells for 4–5 d in a CO2 incubator, the cell culture medium was gently removed, and 100 μL cell proliferation regent WST-8 was added to each well. Following 1–6 h incubation in the CO2 incubator, the absorbance wavelength at 450 nm with correction at 650 nm was measured using a Microplate Reader (Synergy H4 Hybrid Reade, BioTek). The concentration at which 50% inhibition occurred, defined as the IC50, was determined by the sigmoid curve fitting using GraphPad Prism 8.0 (GraphPad, Inc). The seeding density, maintaining time, and incubation time for each cell line were provided in Supplementary Table 3.

Colony formation assay

Resuspended cells were seeded in 6-well plates at a density of 200 cells/well. KH-3 or DMSO (vehicle control) was added to the medium at the same time. On day 5, 0.5 mL FBS was added to each well. Cells were maintained for 14 days in a humidified CO2 incubator. Subsequently, the medium was removed, and the cells were gently washed with PBS buffer before being stained with crystal violet. The number of colonies (with over 50 cells/colony) per well was manually counted. The plating efficiency was calculated based on the following equation: $plating\ efficiency = \frac{Colony\ number\ (treat)}{Colony\ number\ (control)}$.

Western blot analysis

The protein samples (30 μg) were separated by electrophoresis and transferred onto the polyvinylidene difluoride membrane as described before [30]. The membrane was then blocked with the EveryBlot Blocking Buffer (Bio-Rad, cat# 12,010,020) for 40 min at room temperature. Subsequently, the membrane was probed with a primary antibody overnight at 4 °C, followed by incubation with a fluorescence-labeled or HRP-conjugated secondary antibody for 1 h at room temperature. Protein-specific fluorescence/ chemiluminescence was determined by the Odyssey Fc Imaging System (LI-COR Biosciences). All the antibodies used in this study were listed in Supplementary Table 4–5.

RNP-IP

The ribonucleoprotein immunoprecipitation (RNP-IP) was performed as described before [30] with a few modifications. Cells were harvested and lysed following the same protocol described in the protein extraction section, with the addition of the RNase inhibitor to preserve RNA integrity. The protein lysate was then subjected to the RNP-IP assay. The HuR- or control IgG-bounded RNA was extracted from the immunoprecipitated complexes and stored at -80 °C, pending further RT-qPCR analysis.

Cell viability assay

Cells were stained with AO/PI solution (Nexcelom Bioscience, cat# CS2-0106-5 mL) to determine cell viability, following the manufacturer's suggested protocol with a few modifications. Briefly, cells were harvested by trypsinization and centrifugation and resuspended with DMEM medium. Twenty-five μL AO/PI staining solution was mixed with 25 μL of the cell suspension by pipetting up and down. Twenty μL of the mixture was loaded into a counting chamber and the cell viability was determined using a cell counter following the users' guidelines (Cellometer Vision, Nexcelom Bioscience).

DNA and siRNA transfection

The generation of the MDA-MB-231 cell line, which was stably transduced with HuR shRNA, has been previously described [31]. The initiation of HuR shRNA expression was prompted by supplementing the cell culture medium

with doxycycline (1 μg/mL). To perform siRNA transfection, the siRNA smart pool targeting *ELAVL1* (HuR) (Dharmacon Reagents, cat# L-003773–00-0005) or *CFLAR* (cFLIP) (Dharmacon Reagents, cat# L-003772–00-0005) was introduced into cells using Lipofectamine 3000 Reagent (Invitrogen, cat# L3000-015) according to the recommended protocol. The pcDNA3.1-C-(k)DYK vector carrying human *CFLAR* cDNA (transcript variant 1, mRNA, NM_003879.7) ORF was obtained from GenScript and introduced into cells using Lipofectamine 3000 Reagent as per the suggested protocol. In short, cells were seeded on the first day. The following day, the old medium was replaced with fresh medium before transfection, and cells were further maintained for 2–3 days. Regarding drug treatment, the drug was introduced into the medium one day after transfection.

Time-lapse live-cell imaging

The EVOS cell imaging system (EVOS FL Auto, Thermo Fisher, USA) was utilized to monitor the morphology of cells. Briefly, cells were maintained in the on-stage incubation (6% CO2, 37 °C) and images of cells were taken automatedly every 20 min.

Animal tumor models

Five-week-old, male athymic NCr-nu/nu mice, or seven to eight-week-old male NSG mice were purchased from Charles River Laboratories (Wilmington, MA) and Jackson Laboratory (Bar Harbor, ME), respectively. Suspended human prostate cancer cell line PC3 cells (1×10^6 cells) were injected subcutaneously into the flank of both sides of each mouse. Mice were randomized into two groups with 12 tumors/group when the average size of PC3 xenografts reached around 50 mm^3. The anti-tumor effects of KH-3 were also tested using a castration-resistant prostate cancer (CRPC) patient-derived xenograft (PDX), purchased from Jackson Laboratory (TM00298). PDX was implanted into the left flank of each mouse. Mice were randomized into two groups with 10 tumors/group when the average tumor size reached around 100 mm^3. The treatment schedule for the PC3 xenograft model and the PDX model was similar. Each group received one of the following treatments after grouping: 1) KH-3, intraperitoneally (i.p.), QD5×3 or 4 weeks; 2) vehicle control treatment. Once the treatment was initiated, tumor size and body weight were monitored twice a week. The tumor volume was calculated using the length and width of the tumor determined by a caliper: $tumor\ volume = \frac{\text{Length}\times Width^2}{2}$. All the animal experiments carried out in this study were approved by the Institutional Committee for the Use and Care of Animals of the University of Kansas (Authorization # AUS-205–01). Mice were housed in a specific pathogen-free animal facility with free access to standard diet and water. Cages, bedding, and water were autoclaved before use. Experiments would not begin until at least three days after the arrival of the animals.

Statistical analysis

Statistical analysis was conducted using Prism software 8.0 (GraphPad). One-way or Two-way ANOVA test, and t-test were performed to determine statistical differences. Kaplan–Meier analysis followed by a log-rank test was performed to evaluate the tumor growth delay. The specific statistical analysis method, sample size, and number of replicates for each dataset were indicated in the figure legend. $P<0.05$ was considered statistically significant.

Results

The HuR inhibitor KH-3 suppressed cell proliferation and induced apoptosis and autophagy in cancer cells

To assess the cytotoxicity of the HuR functional small molecule inhibitor, KH-3, in different types of cancer cells, multiple cell lines from breast cancer (MDA-MB-231, 2LMP, EMT6) and prostate cancer (PC3, DU145, LNCaP, C42B) were utilized. The results of the MTT-based cytotoxicity assay showed that KH-3 potently inhibited cell viability and proliferation, with IC50 of 2–4 μM in most of the cell lines (Fig. 1A). Furthermore, colony formation assay demonstrated KH-3 induced a dose-dependent decrease in colony numbers of DU145 and PC3 cells (Fig. 1B) as well as of MDA-MB-231 cells [30]. The IC50 of KH-3 for suppressing the plating

(See figure on next page.)

Fig. 1 The HuR inhibitor KH-3 suppressed cell proliferation and induced apoptosis and autophagy in cancer cells. **A** The cell viability curves of breast cancer cells or prostate cancer cells determined by the MTT-based cytotoxicity assay. Cells were treated with KH-3 for 4 days. **B** Representative images of colonies and the colony numbers per well of DU145 and PC-3 cells treated with KH-3. Ordinary one-way ANOVA test, ** $P<0.01$, **** $P<0.0001$. **C** Plating efficiency of cells treated with KH-3 in panel B. The plating efficiency was calculated by the equation: $plating\ efficiency = \frac{Colony\ number\ (treat)}{Colony\ number\ (control)}$. **D** Western blot analysis of whole-cell lysates of multiple cell lines. Breast cancer cells (MDA-MB-231, MCF7). Prostate cancer cells (DU145, LNCaP, and PC3), and the colon cancer cells (HCT116) were treated with 10 μM KH-3 for 24 h before harvesting. GAPDH was used as the loading control. **E** Western blot analysis of DU145 or PC-3 cells treated with KH-3 (5 μM, 10 μM, and 20 μM) or the drug vehicle (DMSO) for 24 h. GAPDH was used as the loading control. All results are presented as mean ± SD of three replicates, unless otherwise specified. All experiments were performed in three repeats, and the representative results were shown

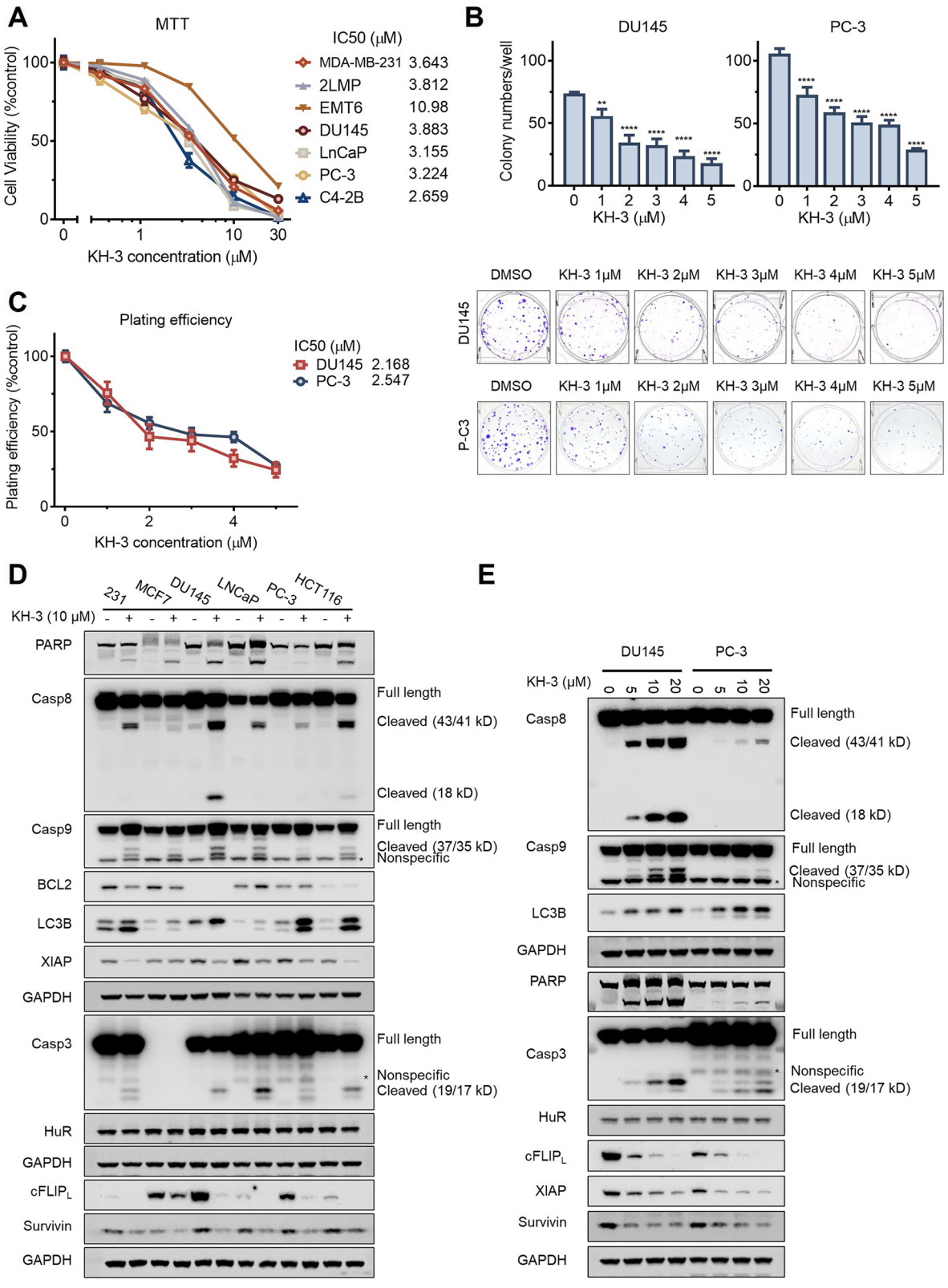

Fig. 1 (See legend on previous page.)

efficiency was 2.168 μM in DU145 cells and 2.547 in PC3 cells (Fig. 1C). In addition, based on real-time morphology monitoring of MDA-MB-231 cells, KH-3 induced the formation of autophagosome after 48 h treatment as indicated by the arrow (Supplementary Fig. 1).

We previously reported that KH-3 induced BCL2-dependent intrinsic apoptosis in breast cancer cells [30]. Interestingly, KH-3 only downregulated the protein levels of BCL2 in MDA-MB-231 and MCF7 cells but not in cells from other cancer types (Fig. 1D). On the other hand, apoptosis can be initiated through the cleavage of Caspase-8, which directly activates downstream caspases, triggering the extrinsic pathway apoptosis pathway [32]. KH-3 treatment reduced the protein levels of cFLIP, XIAP, and Survivin (Fig. 1D). Consequently, apoptotic cell death protein markers, including the activated cleaved forms of Caspase-8, -9, and -3, as well as cleaved PARP, were increased in all tested cells (MDA-MB-231, MCF7, DU145, LNCaP, PC-3, HCT116) upon KH-3 treatment (Fig. 1D).

We then confirmed those findings in DU145 and PC-3 cells with multiple doses of KH-3 treatment (Fig. 1E). At the lowest dose of KH-3 (5 μM) treatment, there was a reduction in cFLIP, XIAP, and Survivin levels, alongside a slight induction of visible cleavage in Caspase-8, Caspase-9, Caspase-3, and PARP in both DU145 and PC3 cell lines. Higher doses of KH-3 resulted in the depletion of cFLIP and XIAP, accompanied by increased cleavage of Caspase-8, Caspase-9, Caspase-3, and PARP. Furthermore, KH-3 promoted the conversion of LC3B-I (upper band) to LC3B-II (the lipidation form, lower band), indicative of autophagosome formation, in a dose-dependent manner (Fig. 1D-E).

Taken together, the above results show that HuR inhibitor KH-3 suppresses cell proliferation and cell viability, as well as induces apoptosis in multiple cancer cell types, including breast, prostate, and colon cancer cells. Therefore, HuR could be a promising anti-cancer therapeutic target across a broad range of cancer types.

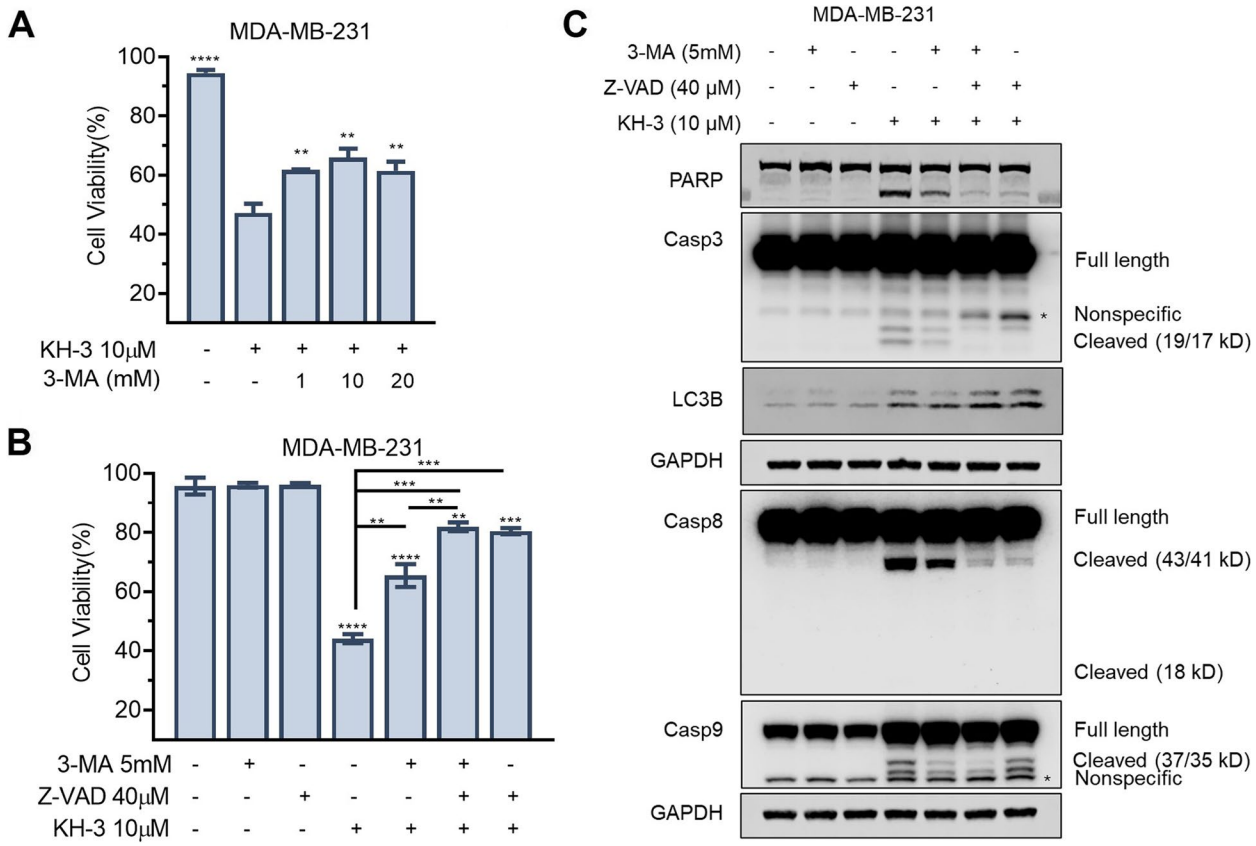

Fig. 2 KH-3 induced autophagy-associated apoptotic cell death. **A** Viability of MDA-MB-231 cells treated with 10 μM KH-3 for 48 h. Cells were pretreated with 3-MA (1, 10, or 20 mM) for 1 h before KH-3. The cell viability was determined by AO/PI staining assay. Ordinary one-way ANOVA test, ** $P < 0.01$, **** $P < 0.0001$ ($n = 2$). **B** Viability of MDA-MB-231 cells treated with KH-3 for 48 h. Before KH-3 treatment, cells were pretreated with 5 mM 3-MA or 40 μM Z-VAD-FMK for 1 h. Ordinary one-way ANOVA test, ** $P < 0.01$, *** $P < 0.001$, **** $P < 0.0001$ ($n = 2$). **C** Western blot analysis of whole-cell lysates of MDA-MB-231 cells receiving the same treatment for 24 h in panel **B**. GAPDH was used as the loading control. Results are presented as mean ± SD of two replicates. All experiments were performed in three repeats, and the representative results were shown

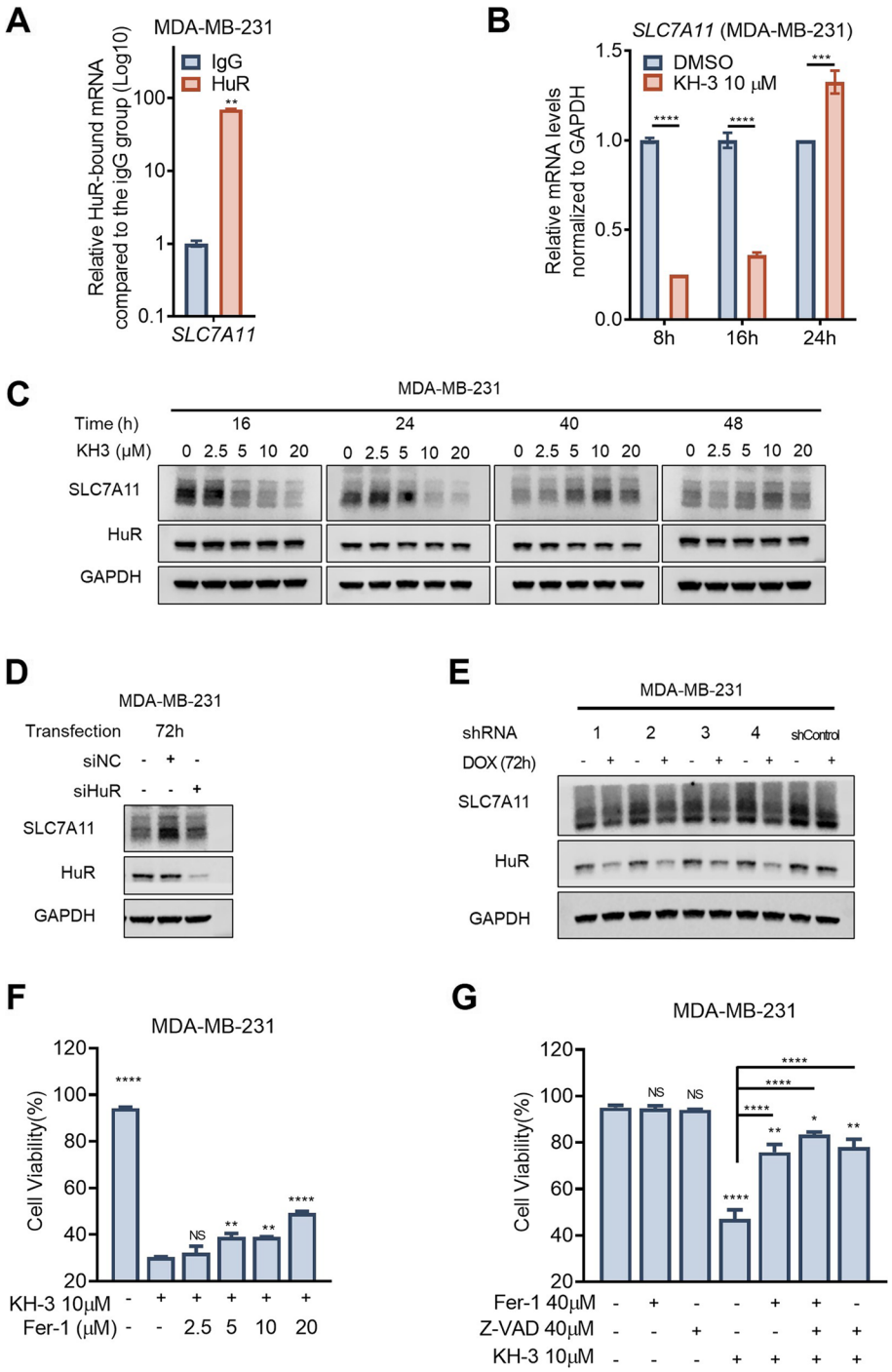

Fig. 3 KH-3 attenuated SLC7A11 and induced ferroptosis. **A** RNP-IP analysis of *SLC7A11* mRNA bound by HuR. Whole-cell lysates form MDA-MB-231 cells underwent RNP-IP, followed by RT-qPCR analysis. RNA enrichment in HuR IP was compared to that in the control IgG IP. Paired t-test test, ** $P < 0.01$ ($n = 2$). **B** RT-qPCR analysis on the RNA levels of *SLC7A11* in MDA-MB-231 cells treated with 10 μM KH-3 for 8 h,16 h, or 24 h. Two-way ANOVA test, *** $P < 0.001$, **** $P < 0.0001$, ($n = 2$). **C** Western blot analysis of whole-cell lysates of MDA-MB-231 cells treated with 10 μM KH-3 for 16, 24, 40, and 48 h. GAPDH was used as the loading control. **D-E** Western blot analysis of whole-cell lysates of MDA-MB-231 cells **D** transfected with HuR siRNA and incubated for 72 h or **E** stably transduced doxycycline inducible HuR shRNA and induced for 72 h. **F-G** Viability of MDA-MB-231 cells treated with 10 μM KH-3 for 48 h. The cell viability was determined by AO/PI staining assay. **F** Cells were pretreated with Ferrostatin-1 (Fer-1) with indicated concentrations for 1 h before adding KH-3. Ordinary one-way ANOVA test, ** $P < 0.01$, **** $P < 0.0001$ ($n = 2$). **G** Before KH-3 treatment, cells were pretreated with 40 μM Fer-1 or 40 μM Z-VAD-FMK for 1 h. Ordinary one-way ANOVA test, * $P < 0.05$, ** $P < 0.01$, **** $P < 0.0001$ ($n = 2$). All results are presented as mean ± SD. All experiments were performed in three repeats, and the representative results were shown

KH-3 induced autophagy-associated apoptotic cell death

Autophagy-dependent cell death is contextual: while autophagy generally promotes cell survival, but it can also lead to cell death [33, 34]. As the above data indicate that KH-3 induces autophagy, we then investigated whether KH-3-induced autophagy lead to cell death or survival by utilizing an autophagy inhibitor, 3-methyladenine (3-MA). Cell viability was significantly decreased by KH-3 treatment compared to the DMSO vehicle control in MDA-MB-231 cells. However, the presence of 3-MA partially restored cell viability in response to KH-3 (Fig. 2A). The off-target activity of 3-MA is reported when using at a high concentration (~10 mM) [35]. Hence, a lower dose of 3-MA was employed to assess the combination effects of autophagy inhibitor (5 mM 3-MA) and caspase inhibitor (40 μM Z-VAD) (Fig. 2B). Both Z-VAD and 3-MA treatments rescued cells from KH-3 induced cell death. The combination treatment further enhanced cell viability compared to the 3-MA treated group, but not to the Z-VAD group.

Western blot analysis was conducted to examine key proteins involved in the apoptosis pathway (Fig. 2C). The KH-3-induced cleavage of Caspase-8, Caspse-9, Caspase-3, and PARP, indicative of apoptotic cell death, was attenuated by both 3-MA and Z-VAD. Notably, the combination of 3-MA and Z-VAD further diminished the cleavage of these proteins induced by KH-3 compared to the 3-MA treatment. The KH-3-induced downregulation of BCL2 and cFLIP (Fig. 1D) might contribute to autophagy [23, 28].

Together, these data show that KH-3 induced autophagy-associated cell death in MDA-MB-231 cells. The autophagy inhibitor 3-MA partially restored cell viability, suggesting that HuR inhibitor KH-3-induced autophagy promotes cell death. Inhibiting both autophagy and apoptosis further restored cell viability. Western blot analysis confirmed that KH-3-triggered apoptosis was reduced by 3-MA. These findings indicate an autophagy-associated apoptotic cell death in parallel with other types of apoptotic cell death following treatment with the HuR inhibitor, KH-3.

KH-3 downregulated SLC7A11 and induced ferroptosis

SLC7A1 is reported to protect cells from ferroptosis [9] and facilitate tumor growth [36]. The RNP-IP result confirmed the direct binding of HuR to the mRNA transcripts of *SLC7A11* in MDA-MB-231 cells (Fig. 3A). The mRNA level of *SLC7A11* was reduced by KH-3 in the early stages of treatment (8 h or 16 h) and showed recovery after 24 h of treatment (Fig. 3B). In addition, this reduction was also reflected at the protein level and exhibited a dose-dependent manner (Fig. 3C).

To confirm that the KH-3 induced reduction in SLC7A11 expression levels was HuR dependent we employed shRNA and siRNA targeting *ELAVL1* (HuR) to modulate HuR expression and assess its impact on SLC7A11. Both the inducible shRNA and the transient siRNA system effectively suppressed HuR protein expression and reduced the protein level of SLC7A11 in MDA-MB-231 cells compared to the negative control siRNA (siNC) or shRNA (shControl) (Fig. 3D-E). Moreover, KH-3 single-agent treatment significantly reduced the cell viability in MDA-MB-231 cells, and the presence of the ferroptosis inhibitor ferrostatin-1 partially restored the cell viability (Fig. 3F-G).

These results show that HuR inhibition, either by the small molecule inhibitor KH-3 or through RNA interference, reduced the RNA and protein levels of *SLC7A11*, suggesting that HuR is a positive regulator for *SLC7A11*. In addition, *SLC7A11* prevents cells from undergoing ferroptosis and promotes tumor growth. Therefore, HuR inhibition could be a promising approach to induce the

(See figure on next page.)

Fig. 4 KH-3 induced apoptosis via suppressing cFLIP. **A** Western blot analysis of cells receiving the same treatments from panel A with different time frames. MDA-MB-231 cells, DU145 cells and PC3 cells were harvested post 48 h transfection. After 1-day post-transfection, 10 μM KH-3 or the drug vehicle was added to the medium. GAPDH was used as the loading control. **B** Cell viability of MDA-MB-23, and DU145 cells transiently transfected with cFLIP siRNA. The AO/PI staining assay was used to measure cell viability. Cells were harvested 3 d post-transfection, and cell viability was determined by the AO/PI staining assay. Viability of cells transfected with siRNA with a non-targeting sequence was served as the negative control (siNC) to provide a baseline reference for the target-specific knockdown. Cell viability of cells treated with 10 μM KH-3 for 48 h was served as the positive control. Ordinary one-way ANOVA test, ** $P < 0.01$, **** $P < 0.0001$ ($n = 2$). **C** Western blot analysis of MDA-MB-231 whole-cell lysates. Cells were harvested 24 h after treatment with 10 μM KH-3. Cells were pretreated with Z-IETD-FMK or Z-VAD for 1 h before the KH-3 treatment. GAPDH was used as the loading control. **D** Cell viability of MDA-MB-231 cells treated with 10 μM KH-3 for 48 h. Cells were pretreated with Z-IETD-FMK (25 μM) for 1 h before adding KH-3. The AO/PI staining assay was used to measure cell viability. Ordinary one-way ANOVA test, ** $P < 0.01$, **** $P < 0.0001$ ($n = 2$). **E** Western blot analysis of the protein levels of cFLIP and other proteins in cell lysates or **F** cell death ratio determined by the AO/PI staining assay of MDA-MB-231 cells. Cells were transiently transfected with control vector or vector containing $cFLIP_L$ ORF. After 24 h of transfection, either the vehicle control (DMSO) or 10 μM KH-3 was added to the medium. Cells were then maintained for an additional 24 h for the Western blot assay or 48 h for the AO/PI staining assay. Ordinary one-way ANOVA test, ** $P < 0.01$, *** $P < 0.001$ ($n = 2$). GAPDH was used as the loading control. Results are presented as mean ± SD. All experiments were performed in three repeats, and the representative results were shown

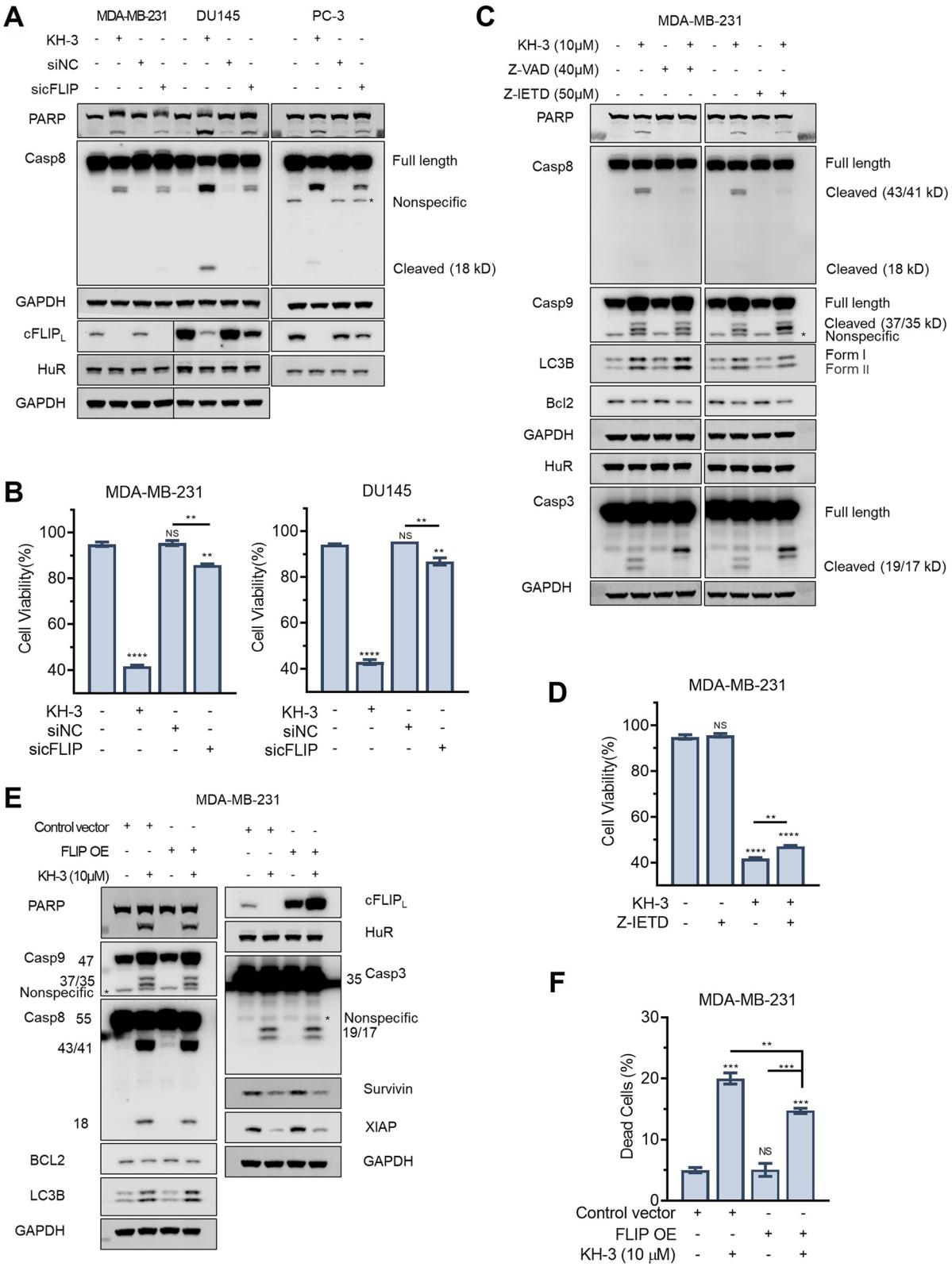

Fig. 4 (See legend on previous page.)

death of cancer cells by suppressing the expression of *SLC7A11* and inducing ferroptosis.

KH-3 induced apoptosis via suppressing cFLIP

cFLIP knockdown triggers the ligand-independent apoptosis, dependent on Caspase-8 and Caspase-7 in the breast cancer cell line MCF-7 [37]. To investigate whether cFLIP depletion induces apoptosis in other cancer cells, the expression of cFLIP was manipulated using siRNA. The protein level of cFLIP was significantly decreased by sicFLIP compared to siNC (Fig. 4B). The downstream proteins of cFLIP-regulated apoptosis, including cleaved Caspase-8 and PARP, were noticeably increased in sicFLIP compared to siNC in MDA-MB-231, DU145, and PC3 cells, (Fig. 4B). The cell viability of MDA-MB-231 and DU145 cells was significantly decreased by siRNA targeting cFLIP (sicFLIP) compared to the negative control siRNA (siNC) (Fig. 4A).

To investigate whether KH-3 induced-cell death was Caspase-8-dependent, a Caspase-8-specific inhibitor, Z-IETD-FMK, was employed to inhibit the activity of Caspase-8. KH-3-induced cleavage of Caspase-8 was nearly depleted by Z-IETD-FMK, and the pan-caspase inhibitor Z-VAD-FMK; the cleavage of PARP was depleted by Z-VAD-FMK but only partially attenuated by Z-IETD-FMK (Fig. 4D). The use of Z-IETD-FMK partially rescued MDA-MB-231 cells from KH-3-induced cell death (Fig. 4C). These data indicate the contribution of other caspase activities to the induction of apoptosis by KH-3 but also suggest the partial Caspase-8 dependence of KH-3-induced apoptosis.

The overexpression of cFLIP (FLIP OE) slightly alleviated the KH-3-induced cleaved-PARP (Fig. 4E) but had no effects on KH-3-induced downregulation of BCL2, Survivin, and XIAP, the increases in LC3B-II, and the cleavage of Caspase-8 (Fig. 4E). Additionally, KH-3-induced cell death was partially decreased by cFLIP overexpression (Fig. 4F).

Taken together, our results suggest that KH-3 induces apoptosis by suppressing cFLIP. Additionally, cFLIP downregulation as well as alternative mechanism(s) are involved in KH-3-induced Caspase-8 activation. On the other hand, it is evident that KH-3 affects other HuR targets (such as BCL2, and XIAP) to regulate cell death.

KH-3 suppressed the growth of prostate *cancer* xenografts

Previously, we reported that KH-3 suppressed the tumor growth of breast cancer [30, 31]. In the current study, we examined the in vivo anti-tumor efficacy of KH-3 in prostate cancer using the PC3-derived xenograft model and the prostate cancer patient-derived xenograft (PDX) model. The growth of PC3 xenografts was significantly suppressed by KH-3 compared to the control treatment (Fig. 5A). At 14 days post-treatment, the average tumor size in the KH-3 treatment group was 55.40% of the control group (Fig. 5B). Kaplan–Meier analysis revealed an increase in the median day for individual tumors to reach 500 mm^3 in the KH-3 group compared to the control group, with median days of 14 and 17, respectively (Fig. 5C). The bodyweight of mice from panel A was shown in Fig. 5D. The images of all tumor tissues collected at the end of the experiment and immunohistochemistry H&E staining of representative tumor tissues were presented in Supplementary Fig. 3. In PC3 xenografts, KH-3 treatment downregulated cFLIP and induced the cleavage of Caspase-3, and PARP (Supplementary Fig. 4A). We also did Western blot analysis of MDA-MB-231 xenografts generated from a previous study [30], which showed that KH-3 downregulate cFLIP and XIAP (Supplementary Fig. 4B).

Furthermore, the results of the prostate cancer PDX (confirmed with high HuR expression, Supplementary Fig. 5) model showed that KH-3 treatment significantly inhibited the tumor growth (Fig. 5E), resulting in over 50% suppression after four-week treatment (Fig. 5F) as compared to that of the control treatment. The median day for tumors to reach 500 mm^3 was significantly delayed from 20 days in the control group to 30.5 days in the KH-3 treatment group (Fig. 5G). The body weight of mice from panel E was shown in Fig. 5H.

(See figure on next page.)

Fig. 5 KH-3 suppressed the growth of prostate cancer xenografts. **A** Growth curves of PC3a xenografts treated with or without KH-3. KH-3 was administered by i.p. injection, 5 times/week × 3 weeks. Two-way ANOVA test, ** $P < 0.01$, **** $P < 0.0001$, $n = 12$. **B** Size of individual tumors for pane **A** at 14 days post-treatment. The ratio of the average tumor size of the treated group normalized to the control group is defined as tumor growth inhibition (T/C %). Multiple t test, ** $P < 0.01$, $n = 12$. **C** Kaplan–Meier analysis of required days for tumor size to reach 500 mm3 from panel **A**. Log-rank test, *** $P < 0.001$, $n = 12$. **D** Average mice bodyweight bearing PC3a xenografts and receiving KH-3 single-agent treatment or the control treatment. **E** Growth curves of prostate cancer PDX treated with or without KH-3. KH-3 was administered by i.p. injection, 5 times/week × 4 weeks. Two-way ANOVA test, * $P < 0.05$, **** $P < 0.0001$, $n = 10$. **F** Size of individual tumors for panel E at 25 days post-treatment. Multiple t test, **** $P < 0.0001$, $n = 10$. **G** Kaplan–Meier analysis of required days for tumor size to reach 500 mm3 from panel E. Log-rank test, **** $P < 0.0001$, $n = 10$. **H** Average mice bodyweight bearing prostate PDX xenografts and receiving KH-3 single-agent treatment or the control treatment. All other results are presented as mean ± SEM

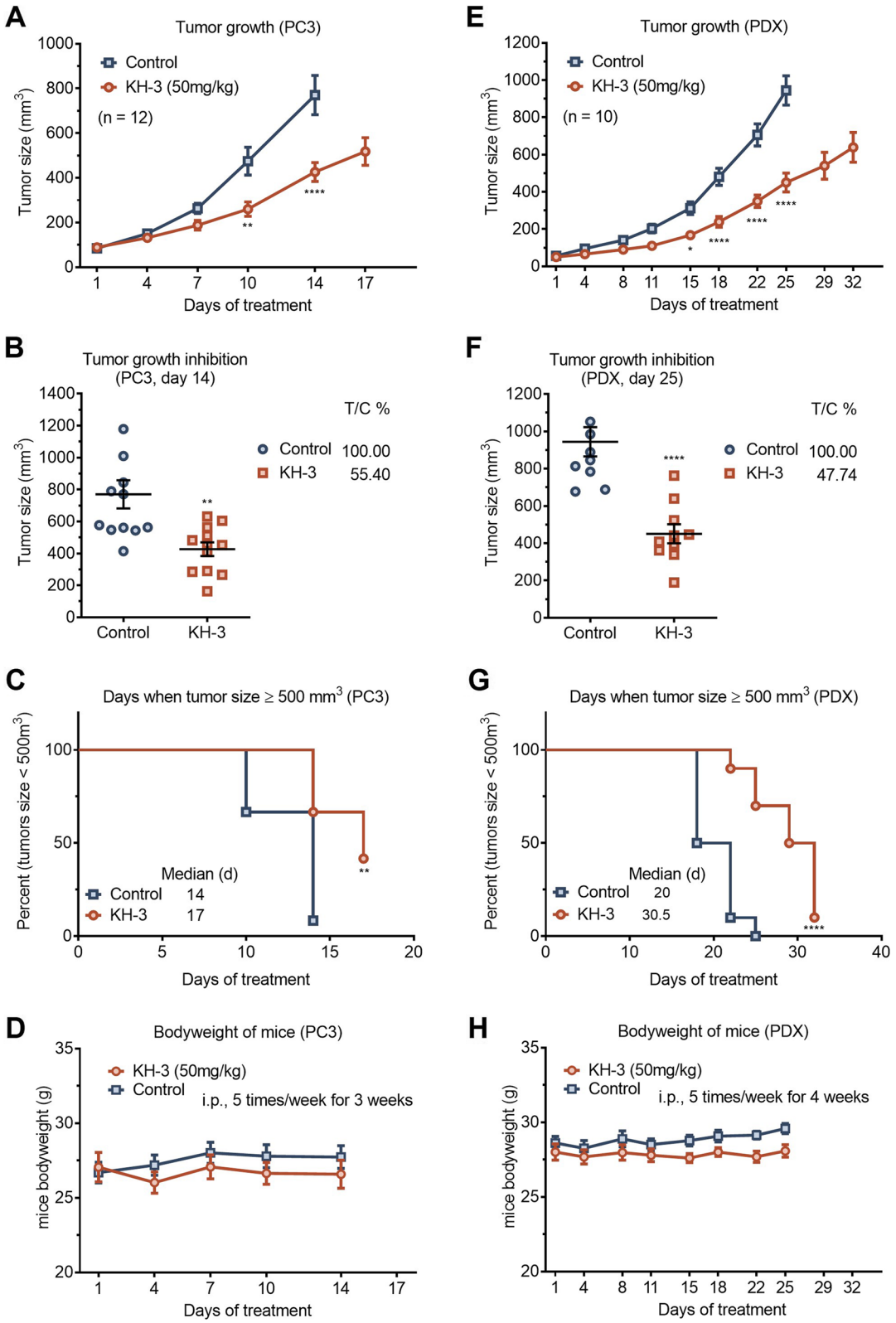

Fig. 5 (See legend on previous page.)

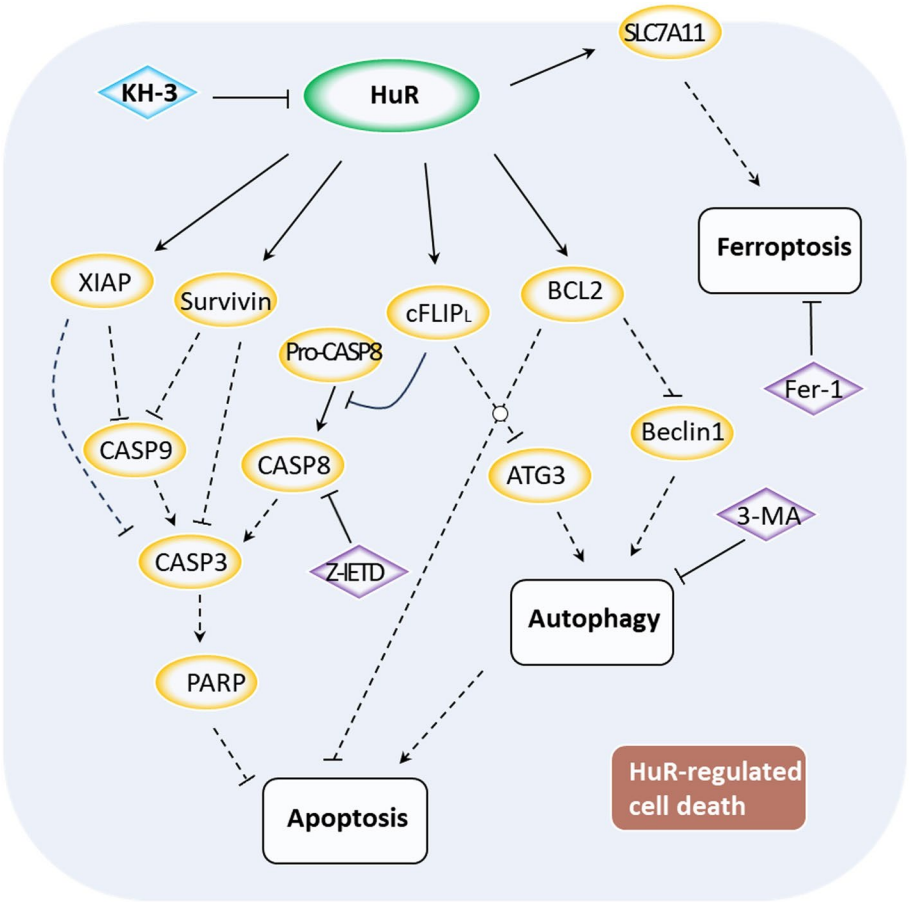

Fig. 6 Proposed working model for the cell death induced by the HuR functional inhibition

These results demonstrate that KH-3 effectively suppresses the growth of prostate cancer models. In PC3 xenografts, KH-3 reduced tumor size by 55% compared to the control and delayed tumor growth. Similarly, in the prostate cancer PDX model, KH-3 treatment resulted in more than 50% tumor suppression and extended the required time for tumors to reach 500 mm^3 by 10 days. These findings highlight the in vivo anti-tumor efficacy of KH-3, supporting its potential as a therapeutic agent for prostate cancer treatment.

Discussion

Understanding the mechanisms underlying cell death upon HuR inhibition in various cellular contexts provides valuable insights into the therapeutic potential of targeting HuR in cancer as well as other pathologies. Our current study explored the anti-tumor effects of HuR functional inhibition, with a specific focus on cell death, using a small molecule inhibitor KH-3. The results demonstrated that KH-3 induced apoptotic cell death in multiple cancer cells as well as autophagy-associated cell death and ferroptosis (Fig. 6). Additionally, KH-3 inhibited tumor growth in two xenograft models of human prostate cancer.

This study reveals that HuR inhibitor, KH-3, induces apoptosis in multiple cancer cells derived from breast, prostate, or colon cancers. Apoptosis can be triggered through the intrinsic pathway tightly regulated by BCL2 or the extrinsic pathway initiated by the death receptor [32, 38]. Therapeutics targeting BCL2, such as BH3 mimics, which neutralize the anti-apoptotic function of BCL2, have been applied to cancer treatment [39]. However, cancer cells with high levels of BCL2 such as PC3 and CL-1, often exhibit resistance to apoptosis [34]. Our findings indicate that the HuR inhibitor KH-3 downregulated cFLIP, leading to the activation of Caspse-8, which triggers extrinsic apoptosis, as well as BCL2-regulated intrinsic apoptosis in various cancer cells. Additionally, KH-3 attenuated protein levels of XIAP and Survivin, resulting in the activation of Caspase-9 and Caspase-3. Therefore, targeting HuR offers an advantage in anticancer strategies: HuR inhibition may induce both intrinsic and extrinsic apoptosis, thereby overcoming BCL2-mediated treatment resistance to cell death.

Our study demonstrates, for the first time, that HuR inhibition downregulates the expression of SLC7A11 in breast cancer. SLC7A11 is considered a therapeutic target for cancer treatment [36]. A recent study has shown that HuR binds to and increases SLC7A11 mRNA stability in gastric cancer cells [24]. SLC7A11 alleviates the ferroptosis-induced ROS and iron accumulation [24], thereby protecting cells from ferroptosis [9] and promoting tumor growth [36]. Our results indicate that inhibiting HuR, either through pharmacological means using KH-3 or through RNA interference, reduces SLC7A11 expression, suggesting that HuR inhibition could be a promising approach to target SLC7A11. However, further investigations are needed to elucidate the downstream events associated with KH-3-induced SLC7A11 inhibition.

Our findings show that KH-3 suppressed the protein levels of cFLIP, and cFLIP knockdown induces apoptosis not only in breast cancer cells in this study and one previous study [37] but also in prostate cancer cells. HuR binds to the mRNA transcripts of cFLIP, XIAP, and Survivin, regulating either their translation levels or mRNA stability [17, 19, 25]. The procaspase-8-cFLIP$_L$ heterodimer leads to the restricted active Capase-8, which inhibits apoptosis and cleaves RIPK1 [27]. However, cFLIP$_L$ overexpression did not significantly attenuate the KH-3-induced cleavage of Caspase-8, suggesting the possible involvement of alternative mechanism(s) employed by KH-3 to activate Caspase-8, which needs to be determined by further investigation. Notably, KH-3 treatment caused the loss of XIAP and BCL2, and enhanced autophagy, compromising the anti-apoptosis effect of cFLIP$_L$ overexpression. These results indicate that the HuR inhibitor KH-3 induces Caspase-8-mediated apoptotic cell death, partially through downregulating cFLIP.

Conclusion

The current study demonstrates the critical role of HuR in suppressing programmed cell death, particularly through post-transcriptionally upregulating cFLIP, XIAP, Survivin, and SLC7A11. These findings underscore the potential of HuR inhibition as a promising anti-tumor strategy for inducing cell death in cancer therapy. By unraveling the intricate mechanisms through which HuR modulates key factors involved in cell survival, this study lays a strong foundation for further exploration of HuR-targeted therapies aimed at tipping the balance toward cell death in cancer cells. This proof-of-concept study underscores the importance of targeting HuR as a viable approach to enhance the efficacy of cancer treatments focused on inducing programmed cell death.

Supplementary Information

The online version contains supplementary material available at https://doi.org/10.1186/s12964-024-01916-z.

Supplementary Material 1: Supplementary Fig. 1. Representative time-lapse images of MDA-MB-231 cells treated with 10 μM KH-3. 40x microscope magnification. Scale bar 100 μM. Supplementary Fig. 2. Western blot analysis of cell lysates of MDA-MB-231 cells. Cells were treated with 10 μM KH-3 from 16 h to 70 h, or with 2.5 μM to 20 μM KH-3 for 24 h. GAPDH was used as the loading control. Supplementary Fig. 3. PC-3 xenografts images. (A) The xenograft model was established by injecting PC-3 cells into mice. At the end of the experiment, tumors were isolated for imaging and subsequent analyses. (B) Images of H&E staining of representative tumor tissues. Supplementary Fig. 4. Western blot analysis of tissue lysates of xenografts. (A) PC3 xenografts from Fig. 5A-D. (B) MDA-MB-231 xenografts described in a previous study. Before harvesting these xenografts, mice were treated with KH-3., which was administered intraperitoneally (i.p.) with 50 mg/kg, QD5 x 4 weeks. GAPDH was used as the loading control. Supplementary Fig. 5. Images of IHC staining of representative PDX donor tissue. For the second PDX model used in this study (Fig. 5E-H), we confirmed the high HuR expression in the donor tissue using IHC staining. Supplementary Table 1. Chemical reagents. Supplementary Table 2. Primers used for the RT-qPCR. Supplementary Table 3. Conditions for MTT-based cytotoxicity assay. Supplementary Table 4. Primary antibody. Supplementary Table 5. Secondary antibody.

Acknowledgements
We thank Dr. Yuxia Zhang from the University of Kansas Medical Center for helping with the immunohistochemistry staining.

Authors' contributions
X.W. and L.X.: conceptualization, supervision, funding acquisition, review, revision, and approval of the manuscript. L.W.: investigation, methodology, validation, original draft preparation, editing, and revision of the manuscript. S.H.K., J.A., and A.A.: investigation, methodology, review, and editing of the manuscript. All authors have approved the final version of this manuscript. All authors have approved the final version of this manuscript.

Funding
This study was supported in part by the National Institutes of Health grants R01 CA191785, CA243445, R33 CA252158, Department of Defense Breast Cancer Research Program Breakthrough Level II grant BC151845, and Kansas Bioscience Authority Rising Star Award (to L.X.); the Susan G. Komen Career Catalyst Research grant CCR18548252, Department of Defense Prostate Cancer Research Program Idea Development Award W81XWH2110573 (to X.W.); the National Cancer Institute Cancer Center Support Grant P30 CA168524.

Data availability
All data supporting the conclusions drawn in this study are provided in the article and its Supplementary Materials. Additional raw data can be acquired by contacting the corresponding author with a reasonable request.

Declarations

Ethics approval and consent to participate
Not applicable.

Consent for publication
Not applicable.

Competing interests
The authors declare no competing interests.

Received: 6 August 2024 Accepted: 30 October 2024
Published online: 03 December 2024

References

1. Kotta-Loizou I, Vasilopoulos SN, Coutts RH, Theocharis S. Current evidence and future perspectives on HuR and breast cancer development, prognosis, and treatment. Neoplasia. 2016;18:674–88.
2. Srikantan S, Gorospe M. HuR function in disease. Front Biosci (Landmark Ed). 2012;17:189–205.
3. Chen CY, Xu N, Shyu AB. Highly selective actions of HuR in antagonizing AU-rich element-mediated mRNA destabilization. Mol Cell Biol. 2002;22:7268–78.
4. Abdelmohsen K, Lal A, Kim HH, Gorospe M. Posttranscriptional orchestration of an anti-apoptotic program by HuR. Cell Cycle. 2007;6:1288–92.
5. Abdelmohsen K, Gorospe M. Posttranscriptional regulation of cancer traits by HuR. Wiley Interdiscip Rev RNA. 2010;1:214–29.
6. Hotchkiss RS, Strasser A, McDunn JE, Swanson PE. Cell Death. N Engl J Med. 2009;361:1570–83.
7. Kepp O, Galluzzi L, Zitvogel L, Kroemer G. Pyroptosis – a cell death modality of its kind? Eur J Immunol. 2010;40:627–30.
8. Linkermann A, Green DR. Necroptosis. N Engl J Med. 2014;370:455–65.
9. Dixon SJ, Lemberg KM, Lamprecht MR, Skouta R, Zaitsev EM, Gleason CE, Patel DN, Bauer AJ, Cantley AM, Yang WS, et al. Ferroptosis: an iron-dependent form of nonapoptotic cell death. Cell. 2012;149:1060–72.
10. Vorobjeva NV, Chernyak BV. NETosis: Molecular mechanisms, role in physiology and pathology. Biochemistry (Mosc). 2020;85:1178–90.
11. Liu X, Nie L, Zhang Y, Yan Y, Wang C, Colic M, Olszewski K, Horbath A, Chen X, Lei G, et al. Actin cytoskeleton vulnerability to disulfide stress mediates disulfidptosis. Nat Cell Biol. 2023;25:404–14.
12. Blanco FF, Jimbo M, Wulfkuhle J, Gallagher I, Deng J, Enyenihi L, Meisner-Kober N, Londin E, Rigoutsos I, Sawicki JA, et al. The mRNA-binding protein HuR promotes hypoxia-induced chemoresistance through posttranscriptional regulation of the proto-oncogene PIM1 in pancreatic cancer cells. Oncogene. 2016;35:2529–41.
13. Eberhardt W, Nasrullah U, Haeussler K. Inhibition of Caspase-2 translation by the mRNA binding protein HuR: a novel path of therapy resistance in colon carcinoma cells? Cells. 2019;8.
14. Winkler C, Doller A, Imre G, Badawi A, Schmid T, Schulz S, Steinmeyer N, Pfeilschifter J, Rajalingam K, Eberhardt W. Attenuation of the ELAV1-like protein HuR sensitizes adenocarcinoma cells to the intrinsic apoptotic pathway by increasing the translation of caspase-2L. Cell Death Dis. 2014;5:e1321–e1321.
15. Badawi A, Hehlgans S, Pfeilschifter J, Rödel F, Eberhardt W. Silencing of the mRNA-binding protein HuR increases the sensitivity of colorectal cancer cells to ionizing radiation through upregulation of caspase-2. Cancer Lett. 2017;393:103–12.
16. Katsanou V, Milatos S, Yiakouvaki A, Sgantzis N, Kotsoni A, Alexiou M, Harokopos V, Aidinis V, Hemberger M, Kontoyiannis DL. The RNA-binding protein Elavl1/HuR is essential for placental branching morphogenesis and embryonic development. Mol Cell Biol. 2009;29:2762–76.
17. Durie D, Lewis SM, Liwak U, Kisilewicz M, Gorospe M, Holcik M. RNA-binding protein HuR mediates cytoprotection through stimulation of XIAP translation. Oncogene. 2011;30:1460–9.
18. Obexer P, Ausserlechner MJ. X-linked inhibitor of apoptosis protein–a critical death resistance regulator and therapeutic target for personalized cancer therapy. Front Oncol. 2014;4:197.
19. Donahue JM, Chang ET, Xiao L, Wang PY, Rao JN, Turner DJ, Wang JY, Battafarano RJ. The RNA-binding protein HuR stabilizes survivin mRNA in human oesophageal epithelial cells. Biochem J. 2011;437:89–96.
20. Chen X, Duan N, Zhang C, Zhang W. Survivin and tumorigenesis: molecular mechanisms and therapeutic strategies. J Cancer. 2016;7:314–23.
21. Brunelle JK, Letai A. Control of mitochondrial apoptosis by the Bcl-2 family. J Cell Sci. 2009;122:437–41.
22. Shi C-S, Kehrl JH. Bcl-2 regulates pyroptosis and necroptosis by targeting BH3-like domains in GSDMD and MLKL. Cell Death Discovery. 2019;5:151.
23. Marquez RT, Xu L. Bcl-2: Beclin 1 complex: multiple, mechanisms regulating autophagy/apoptosis toggle switch. Am J Cancer Res. 2012;2:214–21.
24. Lin Z, Song J, Gao Y, Huang S, Dou R, Zhong P, Huang G, Han L, Zheng J, Zhang X, et al. Hypoxia-induced HIF-1α/lncRNA-PMAN inhibits ferroptosis by promoting the cytoplasmic translocation of ELAVL1 in peritoneal dissemination from gastric cancer. Redox Biol. 2022;52:102312.
25. Smith CR. HuR contributes to the therapeutic resistance of pancreatic cancer. ProQuest ETD Collection - Thomas Jefferson University; 2016. AAI10124160.
26. Safa AR. Roles of c-FLIP in apoptosis, necroptosis, and autophagy. J Carcinog Mutagen. 2013;Suppl 6.
27. Tsuchiya Y, Nakabayashi O, Nakano H. FLIP the Switch: Regulation of Apoptosis and Necroptosis by cFLIP. Int J Mol Sci. 2015;16:30321–41.
28. Lee JS, Li Q, Lee JY, Lee SH, Jeong JH, Lee HR, Chang H, Zhou FC, Gao SJ, Liang C, Jung JU. FLIP-mediated autophagy regulation in cell death control. Nat Cell Biol. 2009;11:1355–62.
29. Deng B, Wang J, Yang T, Deng Z, Yuan J, Zhang B, Zhou Z, Chen F, Fang L, Liang C, et al. TNF and IFNγ-induced cell death requires IRF1 and ELAVL1 to promote CASP8 expression. J Cell Biol. 2024;223(3):e202305026.
30. Wei L, Zhang Q, Zhong C, He L, Zhang Y, Armaly AM, Aubé J, Welch DR, Xu L, Wu X. Functional inhibition of the RNA-binding protein HuR sensitizes triple-negative breast cancer to chemotherapy. Mol Oncol. 2023;17:1962–80.
31. Wu X, Gardashova G, Lan L, Han S, Zhong C, Marquez RT, Wei L, Wood S, Roy S, Gowthaman R, et al. Targeting the interaction between RNA-binding protein HuR and FOXQ1 suppresses breast cancer invasion and metastasis. Commun Biol. 2020;3:193.
32. Ivanisenko NV, Seyrek K, Hillert-Richter LK, König C, Espe J, Bose K, Lavrik IN. Regulation of extrinsic apoptotic signaling by c-FLIP: towards targeting cancer networks. Trends Cancer. 2022;8:190–209.
33. Denton D, Kumar S. Autophagy-dependent cell death. Cell Death Differ. 2019;26:605–16.
34. Lian J, Wu X, He F, Karnak D, Tang W, Meng Y, Xiang D, Ji M, Lawrence TS, Xu L. A natural BH3 mimetic induces autophagy in apoptosis-resistant prostate cancer via modulating Bcl-2-Beclin1 interaction at endoplasmic reticulum. Cell Death Differ. 2011;18:60–71.
35. Pasquier B. Autophagy inhibitors. Cell Mol Life Sci. 2016;73:985–1001.
36. Koppula P, Zhuang L, Gan B. Cystine transporter SLC7A11/xCT in cancer: ferroptosis, nutrient dependency, and cancer therapy. Protein Cell. 2021;12:599–620.
37. Day TW, Huang S, Safa AR. c-FLIP knockdown induces ligand-independent DR5-, FADD-, caspase-8-, and caspase-9-dependent apoptosis in breast cancer cells. Biochem Pharmacol. 2008;76:1694–704.
38. Bedoui S, Herold MJ, Strasser A. Emerging connectivity of programmed cell death pathways and its physiological implications. Nat Rev Mol Cell Biol. 2020;21:678–95.
39. Labi V, Grespi F, Baumgartner F, Villunger A. Targeting the Bcl-2-regulated apoptosis pathway by BH3 mimetics: a breakthrough in anticancer therapy? Cell Death Differ. 2008;15:977–87.

Publisher's Note

Springer Nature remains neutral with regard to jurisdictional claims in published maps and institutional affiliations.